Korean J. Chem. Eng., 35(1), 137-146 (2018)
DOI: 10.1007/s11814-017-0272-1

pISSN: 0256-1115
eISSN: 1975-7220

High performance removal of methyl mercaptan on metal modified activated carbon

Qiang Liu, Ming Ke†, Pei Yu, Feng Liu, Haiqiang Hu, and Changchun Li

College of Science, China University of Petroleum (Beijing), Beijing 102249, China
(*Received 8 February 2017 • accepted 2 October 2017*)

Abstract−A series of coconut shell activated carbon catalysts, modified by metal oxides, were prepared by an ultrasound-assisted incipient wetness method for the removal of methyl mercaptan (CH_3SH). The catalysts were investigated using XRD, BET, XPS, TEM and TA.The results showed that the catalyst combined with 2 wt% Fe loading and iron (Fe) : copper (Cu) (mole ratio) 10 : 3, and calcination at 300 °C had a superior removal efficiency. The high activity could be attributed to the generation of highly dispersed Fe-Cu nanocomposites. The results revealed that calcination temperature not only influenced the chemical states and nanocomposite size of iron and copper, but also affected the pore structures of the catalysts. Compared with Fe/AC, the interaction between the iron and copper oxides resulted in smaller nanoparticles and high dispersion for Fe-Cu/AC. Product analysis results suggested dimethyl disulfide, metal methanesulfonates and methyl thiolates were the oxidation products which adsorbed on the activated carbon.

Keywords: Methyl Mercaptan, Adsorption/Oxidation, Metal Oxides, Activated Carbon

INTRODUCTION

Mercaptans are highly volatile sulfur compounds well known for the disagreeable odors. Methyl mercaptan is found in natural gas, petroleum gas, and in waste gas produced by industrial and agriculture processes [1,2]. CH_3SH can be oxidized to form sulfate particles, potentially altering the radiative properties of the atmosphere and resulting in the formation of acid rain [3,4]. Furthermore, not only does CH_3SH affect the environment, but it also causes problems within industry. In the synthesis of methanol and ammonia process, the catalyst can be poisoned by trace CH_3SH. Sulfur can poison the catalyst due to its ability to adsorb strongly onto the catalyst surface. In the Fischer-Tropsch process, the catalyst decreases its activity by ca. 50% with 4 mg of sulfur per gram [5]. Thus it is necessary to remove CH_3SH in the feed gas therein.

Many methods have been developed for the removal of CH_3SH, such as adsorption, biological degradation, decomposition, catalytic incineration, photocatalytic oxidation, and catalytic adsorption/oxidation [6-10]. Among these, catalytic adsorption/oxidation is recognized as an effective method for the removal of CH_3SH due to the mild conditions, higher desulfurization efficiency and its low cost.

The application of AC has become more popular for the removal of toxic gas because of the large surface area, highly developed pore structure, and surface chemistry. It was reported that CH_3SH adsorbed on the activated carbon surface could be oxidized to dimethyl disulfide (CH_3SSCH_3) which is stored in the subsequently developed pores [11-13]. Compared with CH_3SH, CH_3SSCH_3 is much more strongly adsorbed at low temperatures because of its larger molecule size and higher boiling point [12,14]. The capacity of AC depends on the pore characteristics and surface chemistry. The adsorption/oxidation of AC was largely affected by the proportion of micropores, especially those with diameters of less than 1nm [15]. Moreover, many previous researchers reported that the removal of CH_3SH can be increased by several functional groups loaded on the activated carbon surface and by the use of metal oxides as the catalytic centers for oxidation [16-22].

At present, most reports are focused on the modification of single metal oxides such as alkali metals, and transition metal oxides. To the best of our knowledge little attention has been paid to the research of the adsorption/oxidation capacity of CH_3SH over bimetallic-based activated carbon, which usually shows synergistic effects in the removal of other toxic gases [23-25]. Herein, we attempt to modify the Fe/AC with copper to develop a more efficient activated carbon for the adsorption/oxidation of CH_3SH. The performance of bimetallic-based catalysts was evaluated by use of CH_3SH breakthrough tests. The roles of water and oxygen were studied by changing the reaction conditions. Thermal regeneration of the exhausted catalysts was also investigated. N_2 adsorption/desorption, X-ray diffraction (XRD), Transmission electron microscopic (TEM) and X-ray photoelectron spectroscopy (XPS) methods were used to study the textural and chemical properties of the catalysts. To explore the mechanism, the reaction productions and properties of the used catalysts were researched using thermal analysis (TA), X-ray photoelectron spectroscopy (XPS) and gas chromatography-mass spectrometry (GC/MS) techniques. As a result of the research, we propose possible reaction pathways occurring on the catalyst surface.

EXPERIMENTAL

1. Catalyst Preparation

Coconut shell activated carbon (AC, 20-40 mesh), which was obtained from Jiangsu Zhuxi New Technology Co., LTD, was used

†To whom correspondence should be addressed.
E-mail: keming@cup.edu.cn

as raw material in the present study. The AC was washed with deionized water and then dried at 115 °C for 12 h. Then the catalysts were prepared by ultrasonic-assisted incipient wetness method. Metal nitrates were used as precursors. AC was impregnated with the appropriate concentration of metal nitrate solution to achieve the certain metal loading. Then the mixtures were treated with ultrasound for 1 h and kept overnight at room temperature. The solutions were heated at 60 °C and stirred until the total evaporation of water. Finally, the prepared samples were dried at 115 °C for 12 h, and then calcined for 4 h in nitrogen atmosphere at a certain temperature (250 °C, 300 °C, 400 °C, or 500 °C). To facilitate the pH decrease caused by the introduction of metal oxides, the samples were stirred in a small volume of 0.01 M NaOH solution for 5 h. The final samples were designated as Fe/AC-T or Fe-Cu/AC-T, where T is referred to as the calcination temperature.

2. Catalyst Characterization

X-ray diffraction (XRD) patterns were obtained with a Panalytical Empyrean diffractometer operated at 40 kV and 40 mA by using Ni-filtered Cu Kα radiation (λ=0.15406 nm). N_2 adsorption-desorption isotherms were performed at 77 K with an Autosorb-iQ (Quantachrome Instruments) surface area analyser. The specific surface area was obtained according to the BET method. The nonlocal density functional theory (NLDFT) mode was used to analyze the results, such as those pertaining to the micropore volume and pore size distribution. X-ray photoelectron spectroscopy (XPS) experiments were measured on a spectrometer (Thermo ESCALAB 250XI, USA) using Al Kα radiation (h_v=1,486.6 eV). The power was 150 W, with a pass energy of 20.0 eV and a step size of 0.1 eV. XPSPEAK 4.1 software was used to analyse the data. Some 0.4 g carbon powder was added with 20 mL water and the mixture was stirred overnight at room temperature. Then the pH of the suspension liquid was denoted as pH of the activated carbon. For the exhausted activated carbons, the pH was designated as pHE. Thermal analysis was performed using a thermal gravimetric analyzer (TGA, Mettler Toledo). The samples were heated at a rate of 10 °C/min in an argon atmosphere with a 50 mL/min flow rate. Some 0.3 g carbon powder and 1 mL methanol was placed in a vial and heated at 60 °C for 1 h. Then the exact composition was analyzed by using a Thermo Fisher DSQ gas chromatograph/mass spectrometer. Transmission electron microscopic (TEM) images of the samples were obtained using a JEM-2100F transmission electron microscope operating with an acceleration voltage of 200 kV. The amounts of iron and copper were determined using atomic adsorption spectrometer (spectrAA220FS, Varian Incorporation) after acid digestion.

3. Catalytic Activity Evaluation

Desulfurization tests were performed in a fixed bed reactor (8 mm internal diameter) to evaluate the capacity of the catalysts for the removal of CH_3SH. A schematic diagram of CH_3SH removal system is shown in Fig. 1. First, moist air was used to pre-humidify the catalyst for 1h and the relative humidity was 80% (at 25 °C). The changes in the sample could be used to estimate the water adsorbed on the catalysts. Methyl mercaptan was diluted with air or nitrogen to 2,000 ppm. A saturator system was used to introduce water and the relative humidity was 80% (at 25 °C). The gas hourly space velocity (GHSV) of the entrance gas was kept at 7,500 h^{-1}. A water-bath was used to maintain the reactor temperature at 25 °C. CH_3SH concentrations of the inlet and outlet gases were analyzed using a GC-6890 gas chromatograph with a PFPD detector. To investigate the influence of conditions on the CH_3SH adsorption process, experiments were also conducted under dry air and dry nitrogen conditions, for which the results are referred to as A and N, respectively. For example, ACA represents AC performed in dry air while ACN represents AC performed in dry nitrogen.The breakthrough test stopped at the removal efficiency

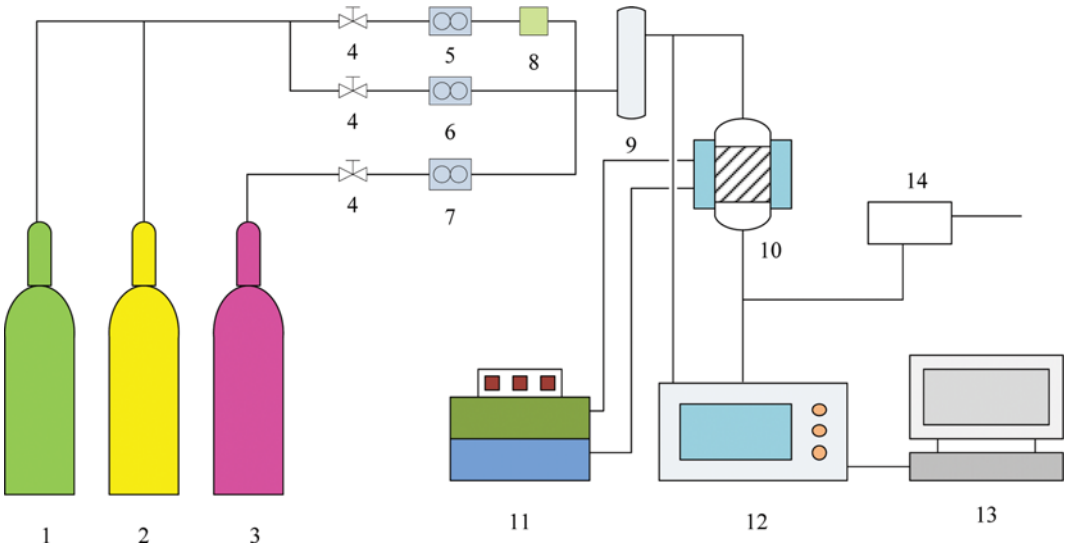

Fig. 1. Schematic diagram of CH_3SH capacity test system.

1. Air cylinder
2. Nitrogen cylinder
3. Methyl mercaptan cylinder
4. Pressure regulator
5. Air flow meter
6. Nitrogen flow meter
7. Methyl mercaptan flow meter
8. Humidifier
9. Mixing column
10. Reactor
11. Cyclic water bath
12. Gas chromatograph
13. Workstation
14. Tail gas adsorber

of 98%. Then the CH_3SH adsorption capacity was obtained according to the follow equations:

$$\alpha = \frac{C_{inlet} - C_{outlet}}{C_{inlet}} \times 100\% \quad (1)$$

$$S = \frac{QC_{inlet}\int_0^t \alpha dt}{m} \quad (2)$$

where C_{inlet} and C_{outlet} are the inlet and outlet CH_3SH concentration in mg/m^3, respectively, α is the removal efficiency, m is the activated carbon weight in g, t is the reaction time in h, Q is the overall gas flow in m^3/h, and S is the CH_3SH adsorption capacity in mg/g.

4. Catalyst Regeneration

The exhausted catalyst was calcined for 1h in nitrogen atmosphere at a certain temperature (300 °C, 400 °C, 450 °C, or 500 °C). To facilitate the pH decrease caused by the deeper oxidation of CH_3SH, the samples were stirred in a small volume of 0.01 M NaOH solution for 5 h. The final samples were designated as R-T, where T refers to the regeneration temperature.

RESULTS AND DISCUSSION

1. Catalytic Performance

1-1. Effect of the Content of Iron on the Adsorption/Oxidation of CH_3SH

Fig. 2 shows the effects of different amounts of iron on the removal of CH_3SH. The best efficiency was achieved at 2.0 wt% addition. In addition, the CH_3SH capacities and actual metal loading amounts of other samples are shown in the supporting information. With the content of iron increasing, the desulfurization efficiency initially increased and then decreased. The results reveal that iron species is the active ingredient for the removal of CH_3SH. The AC impregnated by different amounts of iron has increased the adsorption capacity of CH_3SH to different extent compared with the original AC. When the content of iron was low, CH_3SH could be effectively catalyzed by iron species uniformly dispersed on the surface of the catalyst. However, when the iron loading

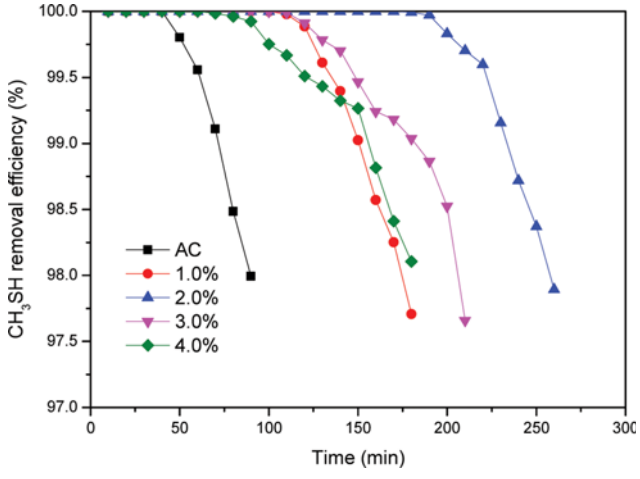

Fig. 2. Effect of the amount of iron on the removal of CH_3SH.

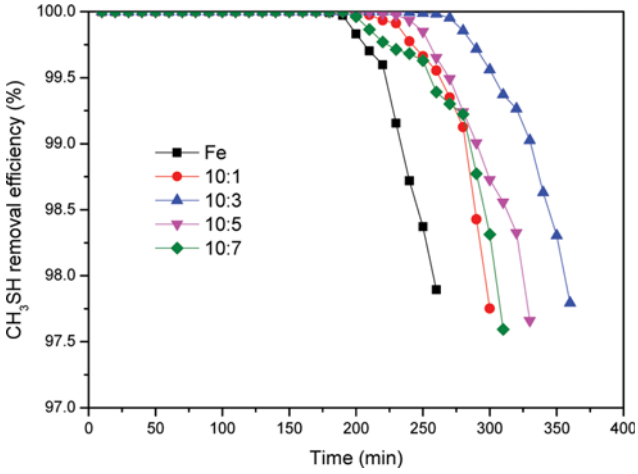

Fig. 3. Effect of the amount of Cu on the removal of CH_3SH.

exceeded a certain threshold, the excessive iron species blocked the catalyst micropore, leading to a decrease in micropore volume so that the adsorption activity was reduced [26].

1-2. Effect of Cu Loading amount on the Adsorption/Oxidation of CH_3SH

Some previous research indicated that addition of second metal could change the properties of the catalyst, affecting its pore and crystal structure, chemical composition, and chemical structure, all of which influenced the catalytic activity [25,27]. In this work, with 2.0 wt% iron, a series of Fe-Cu/AC catalysts were prepared by adjusting the Fe/Cu mole rates: 10 : 1, 10 : 3, 10 : 5, and 10 : 7. The CH_3SH removal capacities are plotted in Fig. 3. In addition, the CH_3SH capacities and actual metal loading amounts of other samples are shown in supporting information. The results indicate that the adsorption/oxidation capacity was increased with the introduction of Cu compared to that of Fe/AC, and the catalyst with Fe/Cu at 10 : 3 exhibited the highest removal efficiency. However, the adsorption/oxidation of CH_3SH decreased when the Cu content increased sequentially. The results also illustrate that the adsorption capacity does not decrease significantly with Fe/Cu at 10 : 5, which could suggest that the Cu-Fe interaction is in favor of CH_3SH adsorption/oxidation. Meanwhile, the interaction between Fe and activated carbon may be enhanced by the addition of Cu.

1-3. Effect of Calcination Temperature on the Adsorption/Oxidation of CH_3SH

Calcination temperature is an important factor in the catalyst preparation, since the catalytic active sites could form after the calcination process at an appropriate temperature [22]. In this part, the modified AC with 2.0 wt% iron and a Fe : Cu (mole ratio) of 10 : 3 at different calcination temperatures were investigated and the results are shown in Fig. 4. The CH_3SH capacities combined with the actual iron and copper loading amounts are summarized in Table 1. The results reveal that the catalyst calcination at 300 °C has the highest activity of removal of CH_3SH. This is because metal oxides are formed which serve as active sites at this temperature. At lower temperatures, there are not enough active sites formed, possibly due to the loss of only water in the calcination process. However, as the calcination temperature increases, the metal oxide

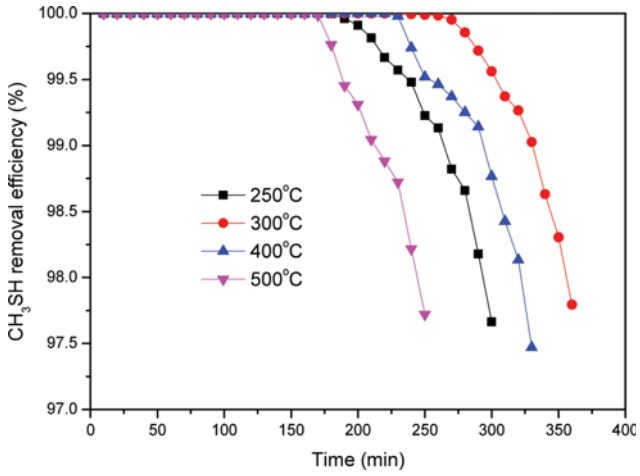

Fig. 4. Effect of calcination temperature on the removal of CH_3SH.

Table 1. CH_3SH capacities and actual metal loading amounts for the samples

Sample	CH_3SH capacity (mg/g)	Metal loading (wt%)	
		Fe	Cu
Fe-Cu/AC-250	380.8	1.98	0.67
Fe-Cu/AC-300	485.2	2.01	0.68
Fe-Cu/AC-400	418.9	1.97	0.68
Fe-Cu/AC-500	317.5	2.06	0.69
Fe/AC-300	341.7	2.03	-

particle size increases and the pore volume shrinks, thus leading to a decreased adsorption capacity. Moreover, the catalytic activity can also be influenced by the crystallinity of the metal oxides.

1-4. Effect of Operation Condition on the Adsorption/Oxidation of CH_3SH

To investigate the effects of oxygen and water on the CH_3SH adsorption/oxidation process, breakthrough tests were also done under dry air and dry nitrogen, respectively. The catalyst combined with 2.0 wt% iron and iron (Fe) : copper (Cu) (mole ratio) 10 : 3,

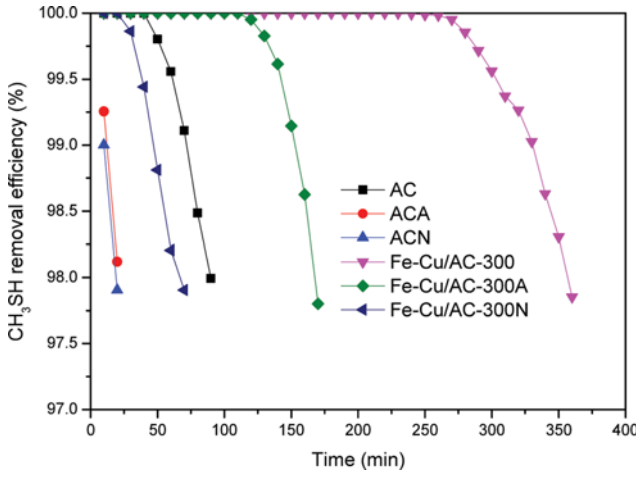

Fig. 5. Effect of operation condition on the removal of CH_3SH.

Table 2. pH of the surface, amount of water pre-adsorbed, and amount of CH_3SH adsorbed for the samples

Sample	pH	pHE	Amount of water (mg/g)	CH_3SH capacity (mg/g)
AC	7.80	7.02	94.7	121.7
ACA	7.80	7.27	0	28.3
ACN	7.80	7.32	0	22.6
Fe-Cu/AC-300	7.84	5.20	102.8	485.2
Fe-Cu/AC-300A	7.84	6.64	0	218.9
Fe-Cu/AC-300N	7.84	6.93	0	92.8

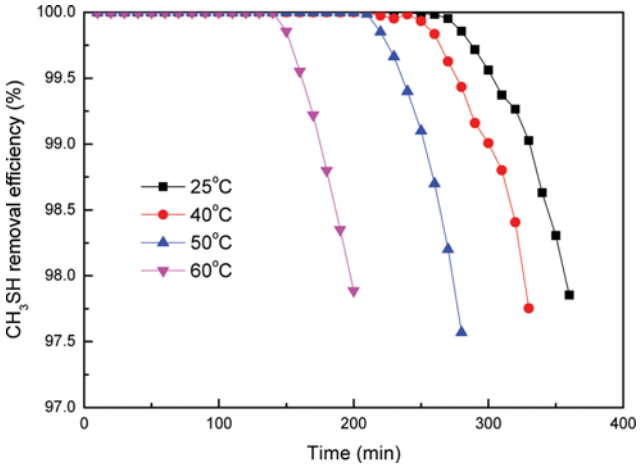

Fig. 6. Effect of reaction temperature on the removal of CH_3SH for Fe-Cu/AC-300.

and calcination at 300 °C was used and the results are collected in Fig. 5 and Table 2. For the original activated carbon, in the absence of moisture, the adsorption/oxidation capacities decreased significantly compared with those running in the moisture feed gas. Moreover, it is interesting to see that the oxygen has different effects upon the removal of CH_3SH on the AC and Fe-Cu/AC-300. The amounts of CH_3SH adsorbed on the AC surface are nearly the same in dry atmosphere whether there is oxygen present or not. However, for Fe-Cu/AC-300, the capacity in dry nitrogen is almost half that measured in the presence of air.

The reaction temperature was further investigated from 25 °C to 60 °C and the results are shown in Fig. 6 and Table 3. Low reaction temperature is favorable for the high removal efficiency. However, it is obvious that the high reaction temperature is deleterious

Table 3. pH of the surface, amount of water pre-adsorbed, and amount of CH_3SH adsorbed for Fe-Cu/AC-300 at different reaction temperature

Reaction temperature (°C)	pH	pHE	Amount of water (mg/g)	CH_3SH capacity (mg/g)
25	7.84	5.20	102.8	485.2
40	7.84	5.11	100.7	435.9
50	7.84	4.92	101.5	373.6
60	7.84	4.71	99.8	271.7

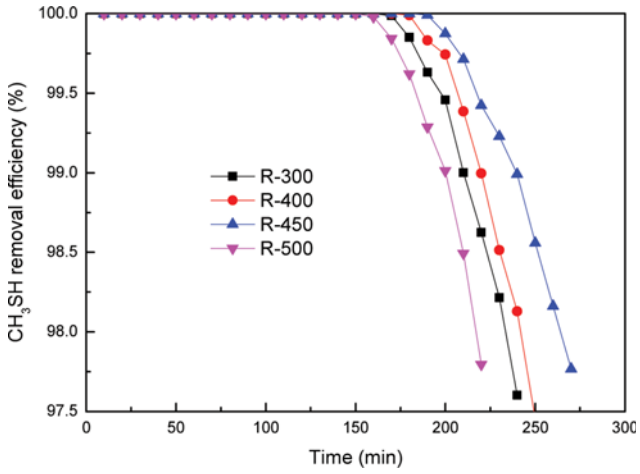

Fig. 7. Effect of thermal regeneration temperature on the removal of CH_3SH.

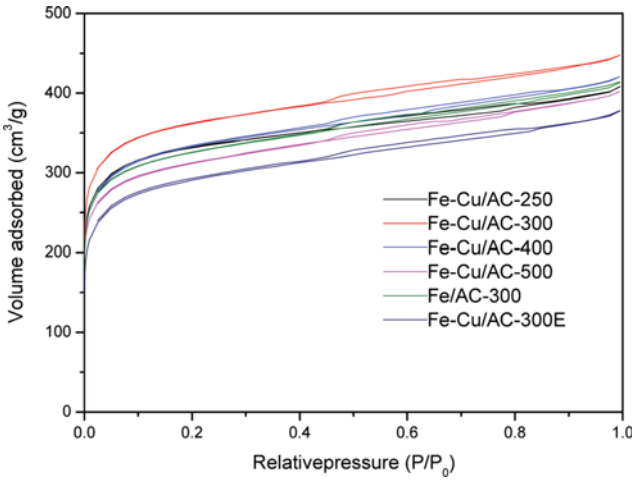

Fig. 8. N_2 adsorption/desorption isotherms of samples.

Table 4. pH of the surface, amount of water pre-adsorbed, and amount of CH_3SH adsorbed for the samples

Sample	pH	pHE	Amount of water (mg/g)	CH_3SH capacity (mg/g)
R-300	7.56	5.82	98.4	318.2
R-400	7.73	5.84	95.2	331.3
R-450	7.85	5.63	90.6	366.8
R-500	7.92	6.21	87.5	300.5

on the catalytic activity. The high temperature may accelerate the formation of deep oxidation products, which may poison the active sites. In addition, the capacity of adsorbing the CH_3SH and O_2 may be weakened with the increase of reaction temperature. Finally, the decrease in the catalytic activity may also be related to the destruction of the water film on the carbon surface when the reaction temperature is high.

1-5. Regeneration of the Exhausted Catalysts

Thermal regeneration was employed to investigate the regeneration performance of Fe-Cu/AC-300 and the results are shown in Fig. 7 and Table 4. It can be deduced that thermal regeneration temperature is an important factor. The best regeneration ability was achieved when the catalyst was regenerated under nitrogen condition at 450 °C. In the adsorption/oxidation process, some deeper oxidation products were generated due to the strong oxidation property of the catalyst. When the thermal regeneration temperature was low, the regeneration ability was low. The reason may be that the deeper oxidation products can be stable under low temperature. However, the regeneration ability also decreased when the temperature was 500 °C. Since the deeper oxidation products may decompose under this condition, the physical and chemical properties of the catalyst were changed under the thermal regeneration process, resulting in the low CH_3SH capacity. Further research of the regeneration process should be performed in the future.

2. Catalyst Characterization

2-1. BET

The N_2 adsorption-desorption isotherms and pore size distribution curves of the representative samples are displayed in Figs. 8 and 9, with the textural parameters calculated being shown in Table 5.

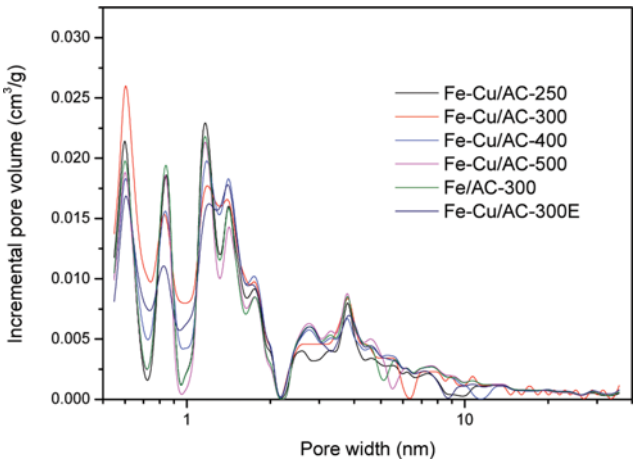

Fig. 9. Pore size distribution curves of samples.

Table 5. Structural parameters of samples calculated from nitrogen adsorption isotherms

Samples	S_{BET} (cm^2/g)	$V_{<1\,nm}$ (cm^3/g)	V_{Micro} (cm^3/g)	V_{Total} (cm^3/g)	V_{Micro}/V_{Total}
Fe-Cu/AC-250	1205	0.273	0.451	0.631	0.715
Fe-Cu/AC-300	1304	0.303	0.486	0.693	0.701
Fe-Cu/AC-400	1215	0.260	0.449	0.650	0.690
Fe-Cu/AC-500	1178	0.257	0.417	0.622	0.670
Fe/AC-300	1232	0.272	0.440	0.640	0.688
Fe-Cu/AC-300E	1110	0.206	0.386	0.584	0.661

Similar isotherm shape is found for all samples, which could be classified as being of type I according to the IUPAC classification. With a sharp knee and a horizontal plateau, the isotherm shape indicates that all samples are mainly microporous materials. Moreover, the hysteresis of the isotherms also indicates the existence of mesopores. A pore size of less than 2 nm is called a micropore while

that <1 nm is named a super-micropore [15]. This is also verified by the pore size distributions of the samples displayed in Fig. 8, in which we can see that the samples are mainly microporous carbons with relatively developed mesopore structures. The textural parameters in Table 5 also indicate that calcination temperatures affect the pore volume and structure. Fe-Cu/AC calcined at 300 °C has the highest specific surface area and largest pore volume. Moreover, the surface area and pore volume decrease as the calcination temperature increases from 300 °C to 500 °C. To study the influence of the addition of Cu on the porous structure, the Fe/AC at 300 °C was also investigated and the surface area and micropore volume decreased. It was reported that the specific surface area and pore structure of the activated carbons are important in the adsorption/oxidation of CH_3SH [11,16,26]. Taking the above desulfurization performance into account, it can be concluded that a high specific surface area and large micropore volume play a crucial role in the removal of CH_3SH. The Fe-Cu/AC-300 after exhaustion was also investigated and above 15.7% decrease is found in the total pore volume, which is mainly attributed to the decreased micropore volume. In combination with the relative high CH_3SH capacity, the probable reason is that the activated carbon is covered with the oxidation products, which most of them can be removed during outgassing in the test process. Moreover, there are still some deeper oxidation products that are adsorbed heavily on the surface.

2-2. XRD

To study the effect of different calcination temperatures, crystal structures of 250 °C, 300 °C, 400 °C and 500 °C were determined by XRD and the XRD patterns are presented in Fig. 10. It was reported that the morphology and amount of metal oxides are weakly affected by calcination temperatures [22,28,29]. However, there are no obvious peaks which can be attributed to crystallite metal oxides for all the samples. The results may suggest that the metal oxides are highly dispersed on the activated carbon surface after calcination. In addition, there are also two other possible explanations. On the one hand, the carbon is non-crystalline and has a strong background peak. On the other hand, there is much less metal oxide present than carbon after calcination. According to the literature, the oxidation state and particle size of the metal oxides are important in the catalytic oxidation process, so other characterization techniques are needed to explore the distinctions of the catalysts caused by different calcination temperatures [15,28].

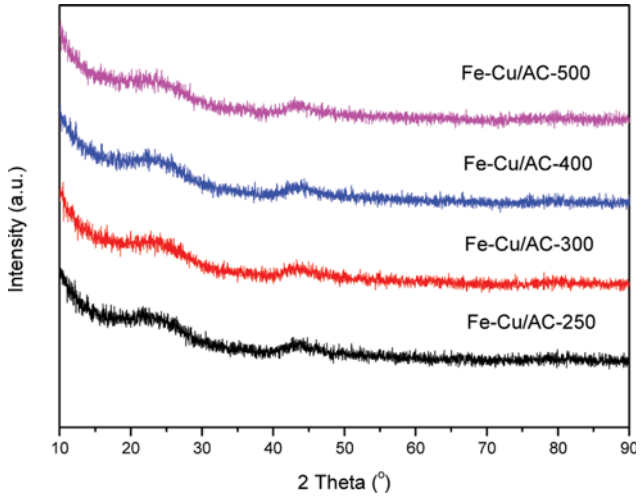

Fig. 10. XRD patterns of Fe-Cu/AC at different calcination temperatures.

2-3. XPS

To understand the chemical states of iron and copper species, the Fe-Cu/AC at different calcination temperatures are characterized by the XPS analysis. The results of Fe 2p XPS spectra are exhibited in Fig. 11. For all the samples, the characteristic peaks of Fe $2p_{3/2}$ and Fe $2p_{1/2}$ are located at 711.8±0.1 eV and 725.3±0.1 eV, which are attributed to the values of Fe_2O_3 [30,31]. In addition, the satellite peak centered at about 729±1 eV for Fe $2p_{3/2}$ also confirms the presence of Fe_2O_3 [28]. Based on the above results, it can be concluded that $Fe(NO_3)_3$ could turn into Fe_2O_3 after the calcination process. Fig. 12 exhibits the XPS spectra of Cu 2p for Fe-Cu/AC-T catalysts. According to the literature, Cu spectra can be divided into two peaks representing Cu^{2+} and (Cu^+ and Cu^0), since

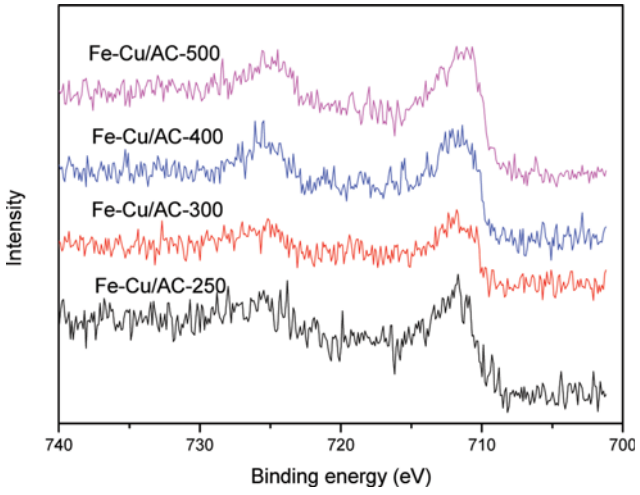

Fig. 11. XPS results of Fe 2p of samples.

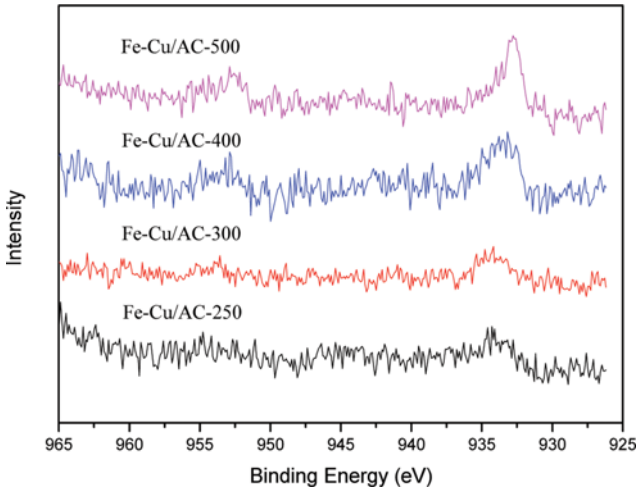

Fig. 12. XPS results of Cu 2p of samples.

Table 6. Surface composition and oxidation state of Cu 2p species over the samples from XPS analysis

Sample	Cu species	
	Cu^{2+}	Cu^{+}/Cu^{0}
Fe-Cu/AC-250	100	0
Fe-Cu/AC-300	100	0
Fe-Cu/AC-400	70.52	29.48
Fe-Cu/AC-500	17.20	82.80

the binding energy of Cu^{+} and Cu^{0} is nearly the same [32]. The results indicate that the characteristic peak at about 934.1±0.1 eV corresponds to Cu^{2+}, and another peak at 932.7±0.1 eV can be attributed to (Cu^{+} and Cu^{0}) [25,32,33]. Table 6 shows the relative surface Cu content calculated from the Cu $2p_{3/2}$ spectra. The results reveal that the Cu species is mainly CuO for the Fe-Cu/AC-250 and Fe-Cu/AC-300. Otherwise, the amount of (Cu^{+} and Cu^{0}) increases with the calcination temperature. The results suggest that CuO dispersed on the carbon surface can be reduced to Cu^{+} or Cu^{0} after high calcination process. In combination with the catalytic activity results, it can be deduced that Fe_2O_3 and CuO are the main active sites for the adsorption/oxidation of CH_3SH.

2-4. TEM

Distributions of the iron and copper species were investigated by the means of TEM experiment, and the results are shown in Fig. 13. Significant differences are observed for the four representative samples. The faint background corresponds to the activated carbon support, while the dark spots belong to iron oxide nanoparticles or Fe-Cu nanoparticles. Spongy porous structure and no obvious dark dots are found for the original activated carbon. However, Fig. 13 also exhibits well-distributed and different sizes of nanoparticles. For the Fe-Cu/AC, when the calcination temperature increases from 300 °C to 500 °C, the average size of Fe-Cu nanoparticles grows sharply from 2.9 nm to 10.4 nm. The results indicate that the Fe-Cu nanoparticles move and aggregate vigorously under high calcination temperature, resulting in larger particle size and poorer distribution. On the other hand, under the same calcination temperature, the average size of Fe-Cu nanoparticles is 2.9 nm on Fe-Cu/AC-300, while the average size of Fe_2O_3 nanoparticles is 4.8 nm on Fe/AC-300. Therefore, it can be concluded that the introduction of copper affects the dispersion of iron species and reduces the aggregation of iron species. In combination with the corresponding desulfurization activity, the size of Fe-Cu nanocomposite is a crucial factor for the adsorption/oxidation of CH_3SH. The reason may be that small particles can be highly dispersed on the carbon surface, providing higher effective contact area between the CH_3SH molecules and active sites. Moreover, it was also reported that a small metal oxide particle itself possesses high catalytic activity due to the nanometer effect [25,29]. However, when the metal oxide particle grows larger, not only are the micropores blocked, but also the effective contact area becomes smaller. Our results are in consistent with the early reports which the small metal oxide particle is beneficial to the removal of NH_3 and SO_2 [15,25].

2-5. Product Analysis

As a result of the research, we propose possible reaction pathways occurring on the catalyst surface. Regarding the process of CH_3SH oxidation on the activated carbon, many researchers think that CH_3SSCH_3 was the major product here [11,34]. In some cases CH_3SSCH_3 could be oxidized into methane sulfonic acid species,

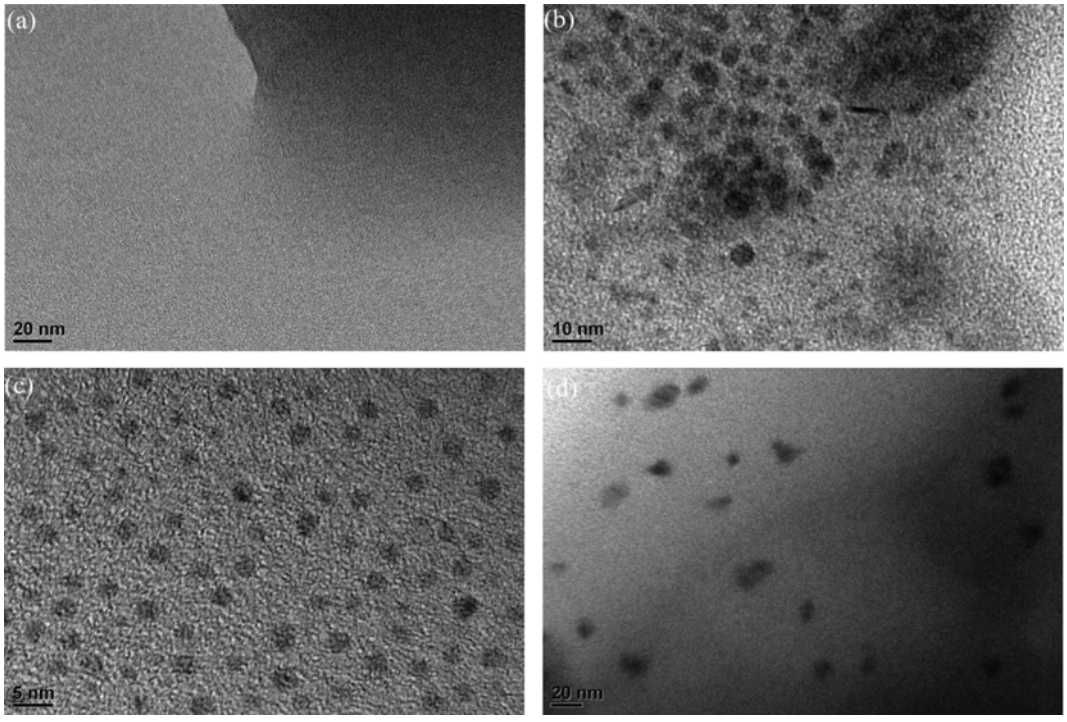

Fig. 13. TEM images of (a) AC, (b) Fe/AC-300, (c) Fe-Cu/AC-300, and (d) Fe-Cu/AC-500.

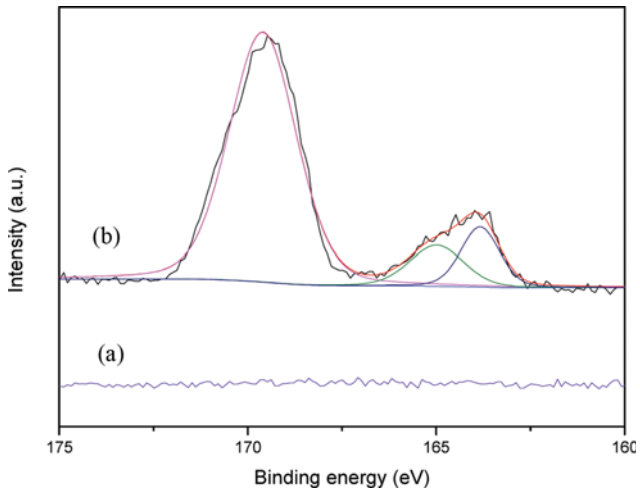

Fig. 14. The S 2p XPS spectra on the samples. (a) Fresh Fe-Cu/AC-300 (b) Exhausted Fe-Cu/AC-300.

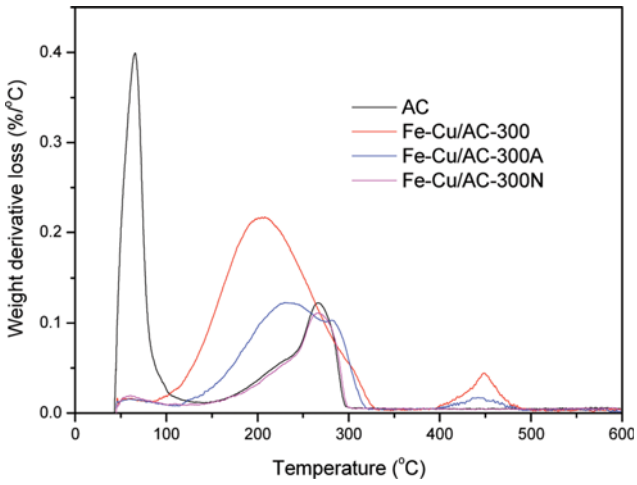

Fig. 15. DTG curves in argon for the exhausted samples.

which damages the active sites. XPS analysis was used to investigate the characteristics of different kinds of these sulfur species on catalyst surfaces. The relevant detailed S 2p XPS results measured on the Fe-Cu/AC-300 and Fe-Cu/AC-300E are shown in Fig. 14. No peaks are observed for the Fe-Cu/AC-300, which suggests that there was no sulfur present in the sample before the desulfurization test. For the Fe-Cu/AC-300E, two same states appear at 163.83 eV and 164.99 eV, which are attributed to methyl thiolate and intact dimethyl disulfide, respectively [34-37]. In addition, the spectrum analysis of Fe-Cu/AC-300E exhibited another peak above 169.60 eV which indicates the production of metal methanesulfonates after the adsorption/oxidation of CH_3SH [22,38]. We infer that CH_3SH was first oxidized to CH_3SSCH_3 by the catalyst and then some of the CH_3SSCH_3 could be converted to metal methanesulfonates and methyl thiolate with the presence of metal oxides and oxygen adsorbed on the catalyst surface. However, the latter two sulfur species which accumulated on the activated carbon surface have bad effects on the catalytic activity.

Thermal analysis (TA) could be used to analyze the sulfur species accumulated on the surface of the exhausted catalysts. A weight loss on the differential thermogravimetry (DTG) curve is indicated as a peak, which the area is in relation to the quantity of the chemical compounds decomposed or removed from the carbon surface at certain temperature [39-41]. To investigate the mechanism of CH_3SH oxidation, the DTG curves were presented for the Fe-Cu/AC-300E exhaustion sample run in different reaction conditions. The DTG curves of representative samples are shown in Fig. 15. The results show that there are two main peaks. Since many researchers think that CH_3SH could only be adsorbed weakly on

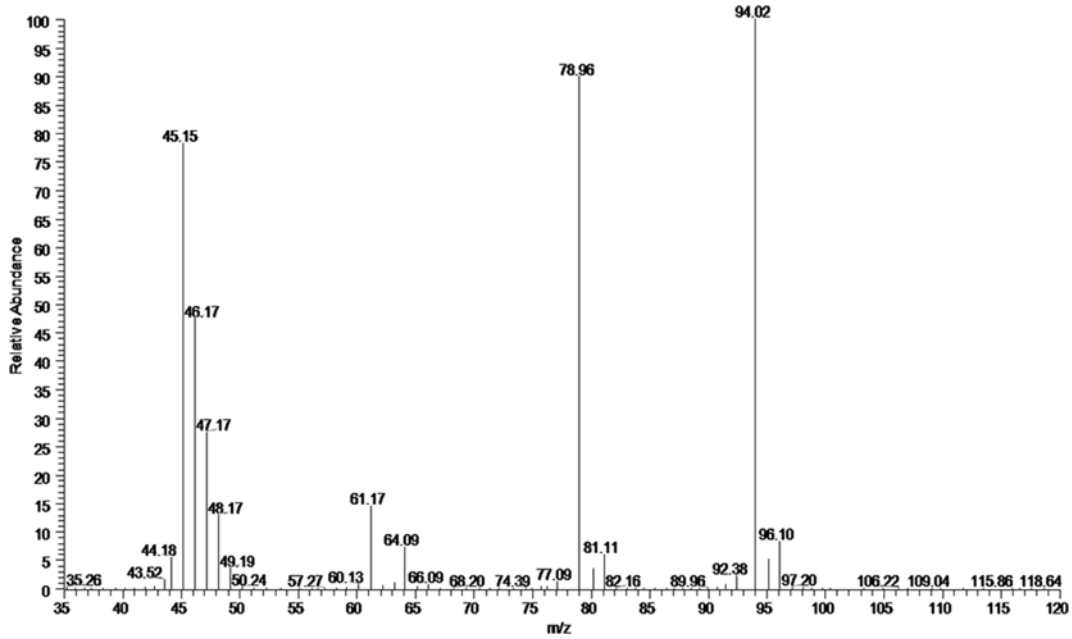

Fig. 16. Mass spectrum for the GC peak detected for the exact from the exhausted Fe-Cu/AC-300.

the carbon surface, it is excluded in the adsorbed phase. The first peak at temperature smaller than 100 °C represents desorption of water [12]. According to the possible reaction route, the peak centered from 100 °C to 300 °C might correspond to the removal of CH_3SSCH_3 [16]. Moreover, there is another peak centered between 400 °C and 450 °C for the Fe-Cu/AC-300 exhaustion sample run in the air conditions regardless of the presence of water. The difference in the Fe-Cu/AC-300 exhaustion sample between the wet air condition and dry air condition is the amount of surface species. Due to the change in pH after exhaustion shown in Table 2, we can determine that the peak represents desorption of small amounts of metal methanesulfonates [42-44]. Otherwise, while the test was run under nitrogen conditions, there was a sharp decrease of the peak centered between 100 °C and 300 °C. Considering that the largest amount of CH_3SH was removed for the Fe-Cu/AC-300 sample running in wet air conditions, the area of the peak from 100 °C to 300 °C is biggest compared to the Fe-Cu/AC sample running under other conditions. It is interesting that there is no peak centered below 100 °C, which indicates that water may be entirely replaced by the abundant CH_3SSCH_3.

GC/MS analysis was used to determine the reaction product extracted from the catalyst with methanol. There is only one peak present on the chromatograms for all samples. Fig. 16 shows the mass spectra for the Fe-Cu/AC-300 under dry air condition, which indicates the existence of CH_3SSCH_3.

The results discussed above suggest that water and oxygen facilitate the CH_3SH adsorption/oxidation process. The reactions occurring on the activated carbon surface could have the following routes [12,40].

$$CH_3SH_g \rightarrow CH_3SH_{ads} \quad (3)$$

$$CH_3SH_{ads} \rightarrow CH_3SH_{ads\text{-}L} \quad (4)$$

$$CH_3SH_{ads\text{-}L} \rightarrow CH_3S^-_{ads} + H^+ \quad (5)$$

$$2CH_3S^-_{ads} + O^{\bullet}_{ads} \rightarrow CH_3SSCH_{3ads} + O^{2-} \quad (6)$$

$$2H^+ + O^{2-} \rightarrow H_2O \quad (7)$$

It was reported CH_3SH could be easily dissociated to form thiolate ions when the pH was greater than 7.6 [40]. In addition, the pH data collected in Table 2 represents the average pH of the carbon surface, which can be different from the pH inside the carbon pores. From the reaction mechanisms discussed above, it is suggested that the concentration of thiolate ions is much greater than the concentration of CH_3SH_{ads} on the activated surface with pH>7.6. So the amount of CH_3SH adsorbed can be increased significantly.

Fe_2O_3 can act as the catalyst site in the adsorption/oxidation of sulfur-containing gas [26]. According to the free-radical mechanism [15], the adsorption/oxidation of CH_3SH on the surface of Fe^{3+} can occur as follows:

$$Fe^{3+} + CH_3S^-_{ads} \rightarrow Fe^{2+} + CH_3S^{\bullet}_{ads} \quad (8)$$

$$2CH_3S_{ads} \rightarrow CH_3SSCH_{3ads} \quad (9)$$

$$Fe^{2+} + O_{2ads} + H^+ \rightarrow Fe^{3+} + HO^{\bullet}_2 \quad (10)$$

$$CH_3S^-_{ads} + HO^{\bullet}_2 \rightarrow CH_3S^{\bullet}_{ads} + HO^-_2 \quad (11)$$

$$HO^-_2 + H^+ \rightarrow H_2O_2 \quad (12)$$

$$2CH_3SH_{ads} + H_2O_2 \rightarrow 2CH_3S^{\bullet}_{ads} + 2H_2O \quad (13)$$

As described above, a redox cycle occurs: Fe^{3+} can promote electron transfer through facilitating the formation of thiolate radicals and the reduction of oxygen. The presence of copper can influence the dispersion of iron species. Moreover, the other role of CuO may be in activation of oxygen for CH_3SH oxidation. Nevertheless, since there are active oxygen radicals and hydroxyl radicals on the activated carbon surface, CH_3SSCH_3 may be further oxidized into methane sulfonate acid species which could react with Fe_2O_3 and CuO. In addition, some of methyl thiolates can also be formed as follows.

$$CH_3S^{\bullet}_{ads} + 3O^{\bullet}_{ads} + H^+ \rightarrow CH_3SO_3H_{ads} \quad (14)$$

$$2xCH_3SO_3H_{ads} + MO_x \rightarrow (CH_3SO_3)_{2x}M + xH_2O \quad (15)$$

$$2xCH_3S^{\bullet}_{ads} + MO_x \rightarrow (CH_3S)_{2x}M + xO^{\bullet} \quad (16)$$

M represents Cu or Fe.

CONCLUSIONS

CH_3SH is a typical sulfur-containing impurity widely distributed in many industrial gases. In this research, a series of activated carbon-based catalysts modified by transition metal oxides were prepared by an ultrasound-assisted incipient wetness method and their activity for the adsorption/oxidation of CH_3SH at room temperature was investigated. The products of CH_3SH oxidation were all adsorbed so strongly on the carbon surface during the adsorption process that only CH_3SH could be found and measured in the outlet gas. The adsorption/oxidation activities results showed that the modified AC with 2.0 wt% iron and a Fe : Cu (mole ratio) of 10 : 3 has superior adsorption/oxidation activity for the removal of CH_3SH. Meanwhile, the calcination temperature also has an obvious effect on the activity and is best at 300 °C. The results indicate that calcination temperature is a crucial factor controlling the oxidation states and nanoparticle sizes of iron and copper species, which affects the adsorption/oxidation capacity. The interaction between iron and copper species leads to the smaller Fe-Cu nanocomposites, higher dispersion and larger micropore volume, which are beneficial to the removal of CH_3SH. Fe_2O_3 and CuO are the most active sites. Moreover, the product analysis results reveal that the main product of CH_3SH oxidation is CH_3SSCH_3. In addition, metal methanesulfonates and methyl thiolates accumulated on the modified activated carbon surface during the adsorption process, which may have negative effects on the adsorption/oxidation of CH_3SH. Regeneration tests indicate that the catalyst can be recovered through thermal treatment and the highest recovered CH_3SH capacity is obtained at 450 °C.

SUPPORTING INFORMATION

Additional information as noted in the text. This information is available via the Internet at http://www.springer.com/chemistry/journal/11814.

REFERENCES

1. L. Ding, T. Liu and X. Li, *J. Chem. Technol. Biot.*, **89**, 455 (2014).
2. M. C. Iliuta and F. Larachi, *J. Chem. Data*, **52**, 2 (2007).
3. M. E. Whelan, D. Min and R. C. Rhew, *Atmos. Environ.*, **73**, 131 (2013).
4. T. Wu, X. Wang, D. Li and Z. Yi, *Atmos. Environ.*, **44**, 5065 (2010).
5. Z. T. Liu, J. L. Zhou and B. J. Zhang, *J. Mol. Catal.*, **94**, 255 (1994).
6. W. Cai, G. Lu, J. He and Y. Lan, *Ceram. Int.*, **38**, 3167 (2012).
7. C. Cammarano, E. Huguet, R. Cadours, C. Leroi, B. Coq and V. Hulea, *Appl. Catal. B.*, **156-157**, 128 (2014).
8. M. G. Conti-Ramsden, K. Nkrumah-Amoako, N. W. Brown and E. P. L. Roberts, *Adsorption*, **19**, 989 (2013).
9. E. Huguet, B. Coq, R. Durand, C. Leroi, R. Cadours and V. Hulea, *Appl. Catal. B.*, **134-135**, 344 (2013).
10. R. C. van Leerdam, P. L. F. van den Bosch, P. N. L. Lens and A. J. H. Janssen, *Environ. Sci. Technol.*, **45**, 1320 (2011).
11. A. Bagreev, J. A. Menendez, I. Dukhno, Y. Tarasenko and T. J. Bandosz, *Carbon*, **43**, 208 (2005).
12. S. Bashkova, A. Bagreev and T. J. Bandosz, *Environ. Sci. Technol.*, **36**, 2777 (2002).
13. K. Hiroshi, K. Isao, H. Mitsuyo and S. Makoto, *Appl. Catal. B.*, **6**, 255 (1995).
14. H. Cui and S. Q. Turn, *Appl. Catal. B.*, **88**, 25 (2009).
15. X. Liu, J. Guo, Y. Chu, D. Luo, H. Yin, M. Sun and R. Yavuz, *Fuel*, **123**, 93 (2014).
16. S. Bashkova, A. Bagreev and T. J. Bandosz, *Langmuir*, **19**, 6115 (2003).
17. D. J. Kim and J. E. Yie, *J. Colloid Interface Sci.*, **283**, 311 (2005).
18. N. Laosiripojana, W. Sutthisripok, S. Charojrochkul and S. Assabumrungrat, *Appl. Catal. A.*, **478**, 9 (2014).
19. S. Lee, W. M. A. W. Daud and M. Lee, *J. Ind. Eng. Chem.*, **16**, 973 (2010).
20. H. Tamai, H. Nagoya and T. Shiono, *J. Colloid Interface Sci.*, **300**, 814 (2006).
21. E. Vega, J. Lemus, A. Anfruns, R. Gonzalez-Olmos, J. Palomar and M. J. Martin, *J. Hazard. Mater.*, **258-259**, 77 (2013).
22. S. Zhao, H. Yi, X. Tang, F. Gao, B. Zhang, Z. Wang and Y. Zuo, *J. Clean. Prod.*, **87**, 856 (2015).
23. X. Wang, J. Qiu, P. Ning, X. Ren, Z. Li, Z. Yin, W. Chen and W. Liu, *J. Hazard. Mater.*, **229-230**, 128 (2012).
24. H. Yi, K. Li, X. Tang, P. Ning, J. Peng, C. Wang and D. He, *J. Chem. Eng.*, **230**, 220 (2013).
25. T. Zhang, J. Liu, D. Wang, Z. Zhao, Y. Wei, K. Cheng, G. Jiang and A. Duan, *Appl. Catal. B.*, **148-149**, 520 (2014).
26. S. Bashkova, A. Bagreev and T. J. Bandosz, *Catal. Today*, **99**, 323 (2005).
27. D. He, H. Yi, X. Tang, P. Ning, K. Li, H. Wang and S. Zhao, *J. Mol. Catal. A-Chem.*, **357**, 44 (2012).
28. J. Guo, X. Liu, D. Luo, H. Yin, J. Li and Y. Chu, *Ind. Eng. Chem. Res.*, **54**, 1261 (2015).
29. Z. Cui, J. Fan, H. Duan, J. Zhang, Y. Xue and Y. Tan, *Korean J. Chem. Eng.*, **34**, 29 (2017).
30. A. Rey, M. Faraldos, J. A. Casas, J. A. Zazo, A. Bahamonde and J. J. Rodriguez, *Appl. Catal. B.*, **86**, 69 (2009).
31. M. Descostes, F. Mercier, N. Thromat, C. Beaucaire and M. Gautier-Soyer, *Appl. Surf. Sci.*, **165**, 288 (2000).
32. G. Zhang, Z. Li, H. Zheng, T. Fu, Y. Ju and Y. Wang, *Appl. Catal. B.*, **179**, 95 (2015).
33. Z. Hu, Y. Zhu, Z. Gao, G. Wang, Y. Liu, X. Liu and Z. Yuan, *Chem. Eng. J.*, **302**, 23 (2016).
34. R. Benassi, *Theor. Chem. Acc.*, **112**, 95 (2004).
35. D. G. Castner, *Langmuir*, **12**, 5083 (1996).
36. D. R. Mullins and T. S. McDonald, *Surf. Sci.*, **602**, 1280 (2008).
37. T. S. Rufael, D. R. Huntley, D. R. Mullins and J. L Gland, *J. Phys. Chem. B.*, **102**, 3431 (1998).
38. Y. Lin, T. Tseng and H. Chu, *Appl. Catal. A.*, **469**, 221 (2014).
39. F. Adib, A. Bagreev and T. J. Bandosz, *J. Colloid. Interf. Sci.*, **214**, 407 (1999).
40. F. Adib, A. Bagreev and T. J. Bandosz, *Environ. Sci. Technol.*, **34**, 686 (2000).
41. A. Bagreev, J. Angel Menendez, I. Dukhno, Y. Tarasenko and T. J. Bandosz, *Carbon.*, **42**, 469 (2004).
42. M. Wang, Z. Wang, Z. Sun and H. Jiang, *React. Kinet. Catal. Lett.*, **84**, 223 (2005).
43. M. Wang, Z. G. Song, H. Jiang and H. Gong, *J. Therm. Anal. Calorim.*, **98**, 801 (2009).
44. Z. Wu, D. B. Dreisinger, H. Urch and S. Fassbender, *Hydrometallurgy*, **142**, 121 (2014).

Supporting Information

High performance removal of methyl mercaptan on metal modified activated carbon

Qiang Liu, Ming Ke†, Pei Yu, Feng Liu, Haiqiang Hu, and Changchun Li

College of Science, China University of Petroleum (Beijing), Beijing 102249, China
(*Received 8 February 2017 • accepted 2 October 2017*)

Table S1. CH_3SH capacities and actual metal loading amounts for the samples

Sample	CH_3SH capacity (mg/g)	Metal loading (wt%)	
		Fe	Cu
1%Fe/AC-300	235.8	1.98	-
2%Fe/AC-300	341.7	2.03	-
3%Fe/AC-300	264.7	3.05	-
4%Fe/AC-300	223.7	3.99	-

Table S2. CH_3SH capacities and actual metal loading amounts for the samples

Sample	CH_3SH capacity (mg/g)	Metal loading (wt%)	
		Fe	Cu
Fe/AC-300	341.7	2.03	-
Fe-Cu/AC-300(10:1)	382.6	1.96	0.23
Fe-Cu/AC-300(10:3)	485.2	2.01	0.68
Fe-Cu/AC-300(10:5)	412.1	1.97	1.14
Fe-Cu/AC-300(10:7)	381.8	2.05	1.61